JOURNAL OF CATALYSIS 150, 434–438 (1994)

NOTE

The Study of Ultrafine Ni–B and Ni–P Amorphous Alloy Powders as Catalysts

The ultrafine amorphous alloy powders have received much attention in recent years (1–15) because the materials combine the features of amorphous and ultrafine powders and have more surface atoms and a higher concentration of coordinately highly unsaturated sites. This is expected to result in more special properties, especially for the catalytic and magnetic recording applications (13–15). However, the investigation on the catalytic properties and the application of these materials have attracted little attention until now. Okamoto *et al.* (16) characterized the surface of Ni–B and Ni–P catalysts prepared by a chemical reduction method with XPS and found that the change in 3*d* electron density on the nickel metal induced by boron or phosphorus will modify the selectivities of the nickel catalyst for hydrogenation reactions. In the present paper, the ultrafine Ni–B and Ni–P amorphous alloy powders were prepared by similar chemical reduction methods, and a comparative study was conducted in order to reveal the differences in thermal stability and catalysis between the two powders and to assess the reasons for the differences exhibited.

The ultrafine Ni–B amorphous alloy powder was prepared by adding dropwise 8 ml of the 2.5 *M* KBH_4 aqueous solution to 100 ml of the 0.1 *M* nickel acetate [$Ni(CH_3COO)_2 \cdot 4H_2O$] ethanol solution under vigorous stirring at 25°C. The black precipitate was washed with 6 ml 8 *M* aqueous ammonia, then washed thoroughly with a large amount of distilled water, followed by an ethanol rinse, and soaked in 99% ethanol. The ultrafine Ni–P amorphous alloy powder was prepared by heating an aqueous solution that consists of 100 g/l nickel acetate [$Ni(CH_3COO)_2 \cdot 4H_2O$], 100 g/l sodium acetate [CH_3COONa], and 100 g/l sodium hypophosphite [$NaH_2PO_2 \cdot H_2O$] at 90°C with a vigorous stirring. The pH of the solution was adjusted to 11 using 2 *M* NaOH aqueous solution. The black precipitate was washed as in the case of the Ni–B powder and also soaked in ethanol. The compositions of the powders determined by inductively coupled plasma (ICP) spectrometry were found to be $Ni_{71.9}B_{28.1}$ (mol%) for Ni–B powder and $Ni_{87.0}P_{13.0}$ (mol%) for Ni–P powder.

The X-ray diffraction (XRD) patterns were recorded in an XRD diffractometer equipped with a rotating anode. The patterns without background subtraction were not smoothed in order to observe the broadening. Differential scanning calorimetry (DSC) measurements were conducted under N_2 (99.99%) atmosphere on a Dupont 9900 computer–thermal analysis system. Before programming began, the Ni–B and Ni–P powders were heated at 90 and 100°C for 30 min, respectively. The numbers of surface nickel atom were measured on a Pulse Chemisorb 2700 apparatus by adsorbing hydrogen on the surface of the sample. Under Ar flow, the sample was heated at 100°C for 1 h, then heated to 300°C, and subsequently cooled to 100°C. The hydrogen was adsorbed at 100°C under H_2 flow (flowing rate is 30 ml/min) for 20 min. In the calculations, the result that the adsorption of hydrogen on the nickel-metalloid amorphous alloy surface is dissociative (17) was used. The morphology and the particle size of the samples were determined by transmission electron microscopy (TEM) performed on a 100CX electron microscope using 100 kV. After an etching of the surface by Ar^+ ions for 20 s, the X-ray photoelectron spectroscopy (XPS) spectra were recorded with a VG ESCALAB MKII photoelectron spectrometer using Mg$K\alpha$ radiation (10 kV and 30 mA). The base pressure in the analyzing chamber was maintained on the order of 10^{-9} Torr. The spectrometer was operated at 20 eV pass energy. The sample was mounted quickly onto a grid attached to a sample holder in the pretreatment chamber, keeping the powder soaked in 99% ethanol to minimize the oxidation of the powder by air. After evacuating the ethanol, the sample was transferred to the analyzing chamber. The catalytic activities of the powders were measured by the hydrogenation of 1,3-cyclopentadiene to cyclopentene at 25°C in 99% ethanol in a reactor with 1.0 MPa initial pressure of hydrogen. The concentration of 1.3-cyclopentadiene is 1.35×10^{-3} mol · dm^{-3}. The hydrogen pressure between 1.0 and 0.4 MPa decreases linearly with time. The reaction rates in Table 1 were calculated from the reaction time during which the pressure decreases from 0.8 to 0.6 MPa.

0021-9517/94 $6.00

TABLE 1

The Catalytic Activities of Ultrafine Ni–B and Ni–P Amorphous Alloy Powders

Catalysts	Surface area[a] ($m^2 \cdot g\ cat^{-1}$)	Numbers of surface Ni atoms ($g\ cat^{-1}$)	Catalytic activities: Reaction rate (mol $H_2 \cdot g\ cat^{-1} \cdot s^{-1}$)	Catalytic activities: TOF (s^{-1})
Ni–B	29.7	4.57×10^{20}	4.68×10^{-4}	0.617
Ni–P	2.78	4.28×10^{19}	6.43×10^{-5}	0.906

[a] Measured by adsorbing hydrogen.

Figure 1 shows the XRD patterns. A broad peak at $2\theta = 45°$ was observed for both Ni–B and Ni–P powders. It is assigned to the amorphous state of nickel–metalloid alloy (18, 19). No distinct peak corresponding to a crystalline phase was seen in the patterns. The disorder range of an amorphous material can be calculated from the FWHM and the position (θ) of the diffraction peak (20). Comparing the FWHM of Ni–B with that of the Ni–P sample, an obvious difference can be observed, which indicates that Ni–B powder has a wider disorder range than Ni–P powder. Figure 2 shows the DSC spectra of the samples. It exhibits three exothermal peaks for Ni–B (see Fig. 2a) and two peaks for Ni–P powder (see Fib. 2b). The crystalline transformation temperature of Ni–B powder is lower than that of Ni–P powder. This reveals that the ultrafine Ni–B amorphous alloy powder has a lower thermal stability than Ni–P powder.

Because of the different metalloid and preparation methods, the distinct differences of the morphology and

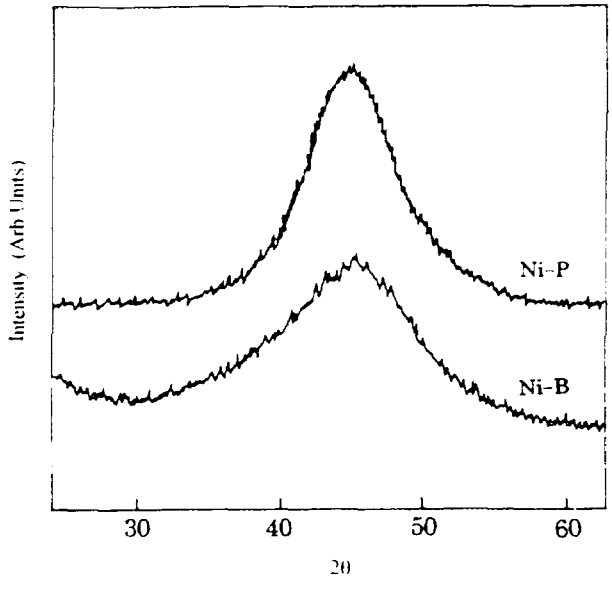

FIG. 1. XRD patterns of Ni–B and Ni–P powders.

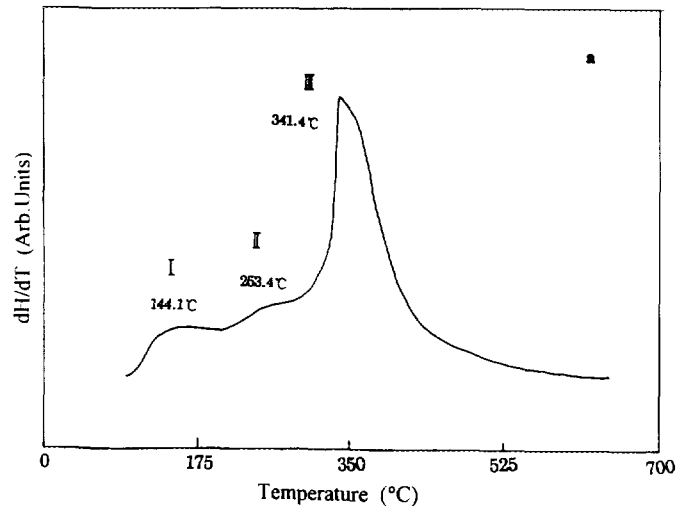

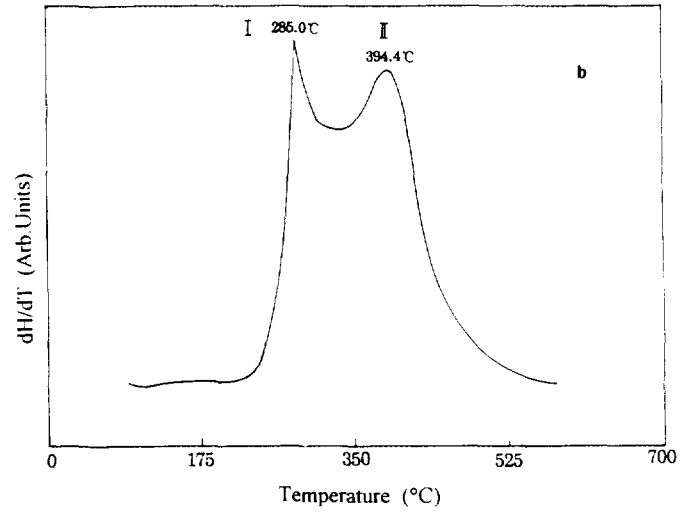

FIG. 2. DSC spectra of Ni–B and Ni–P samples. (a) Ni–B; (b) Ni–P.

particle size between the two samples were observed in TEM micrography (shown in Fig. 3). Ni–P powder has a spherical morphology and the diameter is about 70 nm. The Ni–B powder has a much smaller size, with diameters ranging from 5 to 20 nm, and appears to be interconnected. This is ascribed to the higher surface energy of the small particles. The smaller the particle size, the higher the surface energy of particle. So, the particles tend to connect with each other to reduce the surface energy.

The reaction activities of the hydrogenation of 1,3-cyclopentadiene to cyclopentene catalyzed by ultrafine Ni–B and Ni–P amorphous alloy powders are shown in Table 1. It was found that the reaction rate on Ni–B powder is one order of magnitude more than that on Ni–P

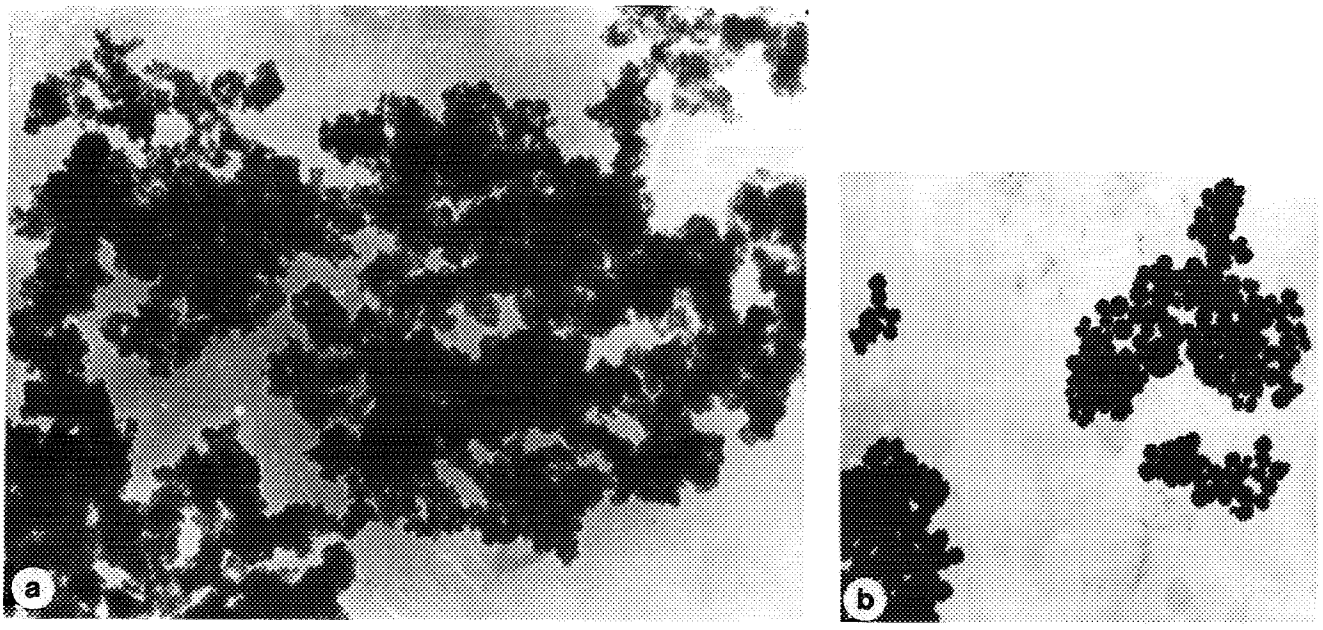

FIG. 3. TEM of Ni–B and Ni–P powders. (a) Ni–B, 1 cm = 70 nm; (b) Ni–P, 1 cm = 250 nm.

powder. The same result was found for the surface area and for the numbers of nickel atoms on surface. Therefore, the turnover frequency (TOF) of hydrogen on Ni–B powder is similar to that on Ni–P powder.

The XPS spectra of the Ni–B powder are shown in Fig. 4a. Compared with the spectrum of pure nickel metal foil, the peak at 852.2 eV in the $Ni_{2p3/2}$ level is ascribed to metallic Ni. In the B_{1s} level, two kinds of boron species appeared. The peaks at the lower and higher binding energy are assigned to boron interacting with nickel (188.0 eV) and oxidized boron (193.2 eV), respectively (16, 21, 22). Compared with the B_{1s} binding energy for elementary boron (186.5–187.0 eV), it is immediately concluded that the boron species interacting with nickel are positively charged, which indicates that the boron donates electrons. The $Ni_{2p3/2}$ signals of Ni–P powder (shown in Fig. 4b) are very similar to those of the Ni–P powder shown in Fig. 4a. The $Ni_{2p3/2}$ binding energy for Ni–P powder is 852.0 eV, consistent with that for pure nickel metal foil and for the nickel metal in Ni–B powder. The evidence from Fig. 4b proves that there exist two kinds of phosphorus on the surface of Ni–P powder. The P_{2p} peak at the binding energy of 133.6 eV is recognized as oxidized phosphorus. The lower binding energy peak at 129.6 eV, shifted negatively by 0.8 eV from red phosphorus (130.4 eV), is assigned to the P bonded to nickel metal on the basis of the similar negative shifts reported for MnP(−0.8 eV) (23), CrP (−1.3 eV) (23), and Cu_3P (−0.4 eV) (24). In contrast with the Ni–B sample, these phosphorus species are negatively charged, which indicates that the phosphorus accepts electrons.

The surface composition calculated from XPS spectra by the analysis of relative peak area is $Ni_{42.4}B_{57.6}$ (mol%) for Ni–B powder and $Ni_{75.9}P_{24.1}$ (mol%) for Ni–P powder. Compared with the bulk composition measured by ICP spectrometry, the metalloids enrich the surface for both samples. However, the enrichment of the metalloid on the Ni–B powder surface is more obvious. On the Ni–B powder surface, the boron species are mostly oxidized. This is different from the phosphorus species on Ni–P powder surface, where the amount of phosphorus bonded to nickel metal is much greater than that which is oxidized. If the content of oxidized metalloid species is subtracted from the surface content of metalloid, the surface composition is $Ni_{81.4}B_{18.6}$ (mol%) for Ni–B powder and $Ni_{82.0}P_{18.0}$ (mol%) for Ni–P powder. They have a similar ratio of nickel atoms to metalloid atoms in this case.

It is evident from the DSC results that ultrafine Ni–B amorphous alloy powder has a lower thermal stability than Ni–P powder, which is due to the difference of metalloid and diameter of particles between the two samples. The ultrafine particles are in a less stable state. The smaller the diameter of the particle, the higher the surface energy, and, hence, the lower the thermodynamic stability. In addition, the process of forming a new crystalline phase in an amorphous phase can be divided into two stages: one is the formation of crystalline nuclei; the other is the growth of the nuclei. The surface of an amorphous alloy can affect the crystallinity by promoting the formation of the crystalline nucleus, because the formation of a new crystalline phase on the surface can reduce the surface energy (25). Since the diameter of the Ni–B parti-

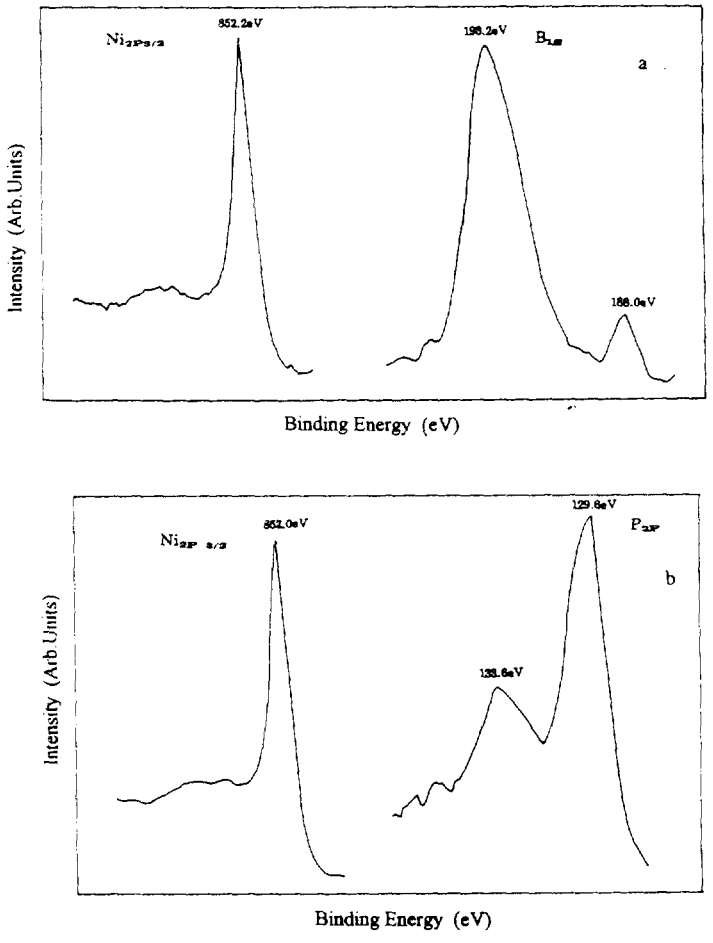

FIG. 4. XPS spectra of Ni–B and Ni–P samples. (a) Ni–B; (b) Ni–P.

cles is much smaller than that of the Ni–P particles, the surface energy of the Ni–B particles is higher than that of the Ni–P particles; the tendency to form a stable crystalline state to decrease the surface energy on the Ni–B particle surface is therefore stronger than that on the Ni–P particle surface. So, the numbers of crystalline nuclei formed in Ni–B powder are much greater than that in Ni–P powder.

The growth of crystalline nuclei in an amorphous alloy is governed by the diffusion rate of the component atoms. The faster it is, the easier the crystallization of the amorphous material is. According to experimental results (26), the diffusion coefficient of boron atom is a few orders of magnitude greater than that of phosphorus atom. This indicates that the diffusion rate of boron in Ni–B powder is faster than that of phosphorus in Ni–P powder. Since Ni–B powder has more crystalline nuclei than Ni–P powder and the boron atom has a faster diffusion rate than phosphorus atom, it can be explained that the thermal stability of Ni–B powder is lower than that of Ni–P powder.

As for the difference of the rate per gram of catalyst between two samples, a good explanation can be given by considering the surface area of the ultrafine particles. Okamoto *et al.* (16) studied the relation between surface characterization and catalytic activity of Ni–B and Ni–P catalysts. They considered that the differences of the catalytic activities are due to the difference of the electron density on the nickel metal between Ni–B and Ni–P catalysts. According to our results, the TOF of hydrogen in the hydrogenation of 1,3-cyclopentadiene on Ni–B powder is similar to that on Ni–P powder. The differences of reaction rate are due to the difference of the active site numbers. Ni–B powder has a smaller size of particle and a bigger surface area (See Table 1) than Ni–P powder; it therefore has a larger ratio of surface atoms to total atoms, which means that it has more active sites. The different electron transference between nickel and metalloid does not result in a distinct change of the electron density on the nickel metal because a distinct difference of $Ni_{2p3/2}$ binding energy between Ni–B and Ni–P powders cannot be observed. It can therefore be concluded that the electronic effect is not the main reason for the differences of the reaction rate per gram of catalyst.

ACKNOWLEDGMENTS

The authors gratefully acknowledge Dr. Zong Baoning and Zhang Dichang, Research Institute of Petroleum Processing, Beijing, People's Republic of China, for their assistance in DSC measurements. This work was supported by the Special Foundation for Doctor Candidate of the State Education Commission of China.

REFERENCES

1. Van Wonterghem, J., Mørup, S., Koch, J. W., Charles, W., and Wells, S., *Nature* **322,** 622 (1986).
2. Van Wonterghem, J. Mørup, S., Meagher, A., Larsen, J., Bentzon, M. D., Clausen, B. S., Koch, C. J. W., Wells, S., and Charles, S. W., *J. Magn. Magn. Mater.* **81,** 138 (1989).
3. Xue, D. S., Li, F. S., and Zhou, R. J., *J. Mater. Sci. Lett.* **9,** 506 (1990).
4. Saida, J., Inoue, A., and Masumoto, T., *Mater. Sci. Eng.* **A133,** 771 (1991).
5. Shen, J. Y., Hu, Z. Zhang, L. F., Li, Y. Z., and Chen, Y., *Appl. Phys. Lett.* **59,** 3545 (1991).
6. Shen, J. Y., Hu, Z., Hsia, Y. F., and Chen, Y., *Appl. Phys. Lett.* **59,** 2510 (1991).
7. Van Wonterghem, J., Mørup, S., Charles, S. W., Wells, S., and Villadsen, J., *Phys. Rev. Lett.* **55,** 410 (1985).
8. Corrias, A., Ennas, G., Licheri, G., Marongiu, G., Musinu, A., Paschina, G., Piccaluga, G., Pinna, G., and Magini, M., *J. Mater. Sci. Lett.* **7,** 407 (1988).
9. Jiang, J., Zhao, F., Gao, D., Dezsi, I., and Gonser, U., *Hyperfine Interact.* **55,** 981 (1990).
10. Jiang, J., Dezsi, I., Gonser, U., and Lin, X., *J. Non-Cryst. Solids* **124,** 139 (1990).
11. Hu, Z., Shen, J. Y., Fan, Y. N., Hsia, Y. F., and Chen, Y., *J. Mater. Sci. Lett.* **12,** 1020 (1993).

12. Shen, J. Y., Hu, Z., Zhang, Q., Zhang, L. F., and Chen, Y., *J. Appl. Phys.* **71,** 5217 (1992).
13. Deng, J. F., and Chen, H. Y., *J. Mater. Sci. Lett.* **12,** 1508 (1993).
14. Yang, J. Chai, L., Deng, J. F., and Zhao, H. L., *Acta Chim. Sin.(Engl. Ed.)* **52,** 53 (1994).
15. Linderoth, S., and Mørup, S., *J. Appl. Phys.* **69,** 5256 (1990).
16. Okamoto, Y., Nitta, Y., Imanaka, T., and Teranishi, S., *J. Chem. Soc., Faraday Trans. 1* **75,** 2027 (1979).
17. Zong, B. N., Min, E. Z., and Deng, J. F., *Chin. J. Mol. Catal.* **4,** 248 (1990).
18. Yamashita, H., Yoshikawa, M., Funabiki, T., and Yoshida, S., *J. Chem. Soc., Faraday Trans. 1* **82,** 1771 (1986).
19. Deng, J. F., Zhang, X. P., and Min, E. Z., *Appl. Catal.* **37,** 339 (1988).
20. Pei, G. W., Zhong, W. L., and Yue, S. B., "X-Ray Diffraction of Single, Crystalline and Amorphous Materials," p. 453. Shandong Univ. Press, Jinan, 1989.
21. Schreifels, J. A., Maybury, P. C., and Swartz, W. E., *J. Catal.* **65,** 195 (1980).
22. Tamaki, J., Takagaki, H., and Imanaka, T., *J. Catal.* **108,** 256 (1987).
23. Pelavin, M., Hendrickson, D. N., Hollander, J. M., and Jolly W. L., *J. Phys. Chem.* **74,** 1116 (1970).
24. Nefedov, V. I., Solyn, Ya. V., Domashevskaya, E. P., Ugai, Ya. A., and Terekhov, V. A., *J. Electron. Spectrosc. Relat. Phenom.* **6,** 231 (1975).
25. Wang, Y. H., and Yang, Y. S., "Amorphous Alloy," p. 113. Metallurgy Industry Press, Beijing, 1989.
26. Wang, Y. H., and Yang, Y. S., "Amorphous Alloy," p. 108. Metallurgy Industry Press, Beijing, 1989.

Jingfa Deng
Jun Yang

Department of Chemistry
Fudan University
Shanghai 200433
People's Republic of China

Shishan Sheng
Hengrong Chen
Guoxing Xiong

National Laboratory of Catalysis
Dalian Institute of Chemical Physics
Chinese Academy of Sciences
Dalian 116023
People's Republic of China

Received January 27, 1994; revised August 3, 1994